# A novel fast imaging modality for free radicals in vivo: continuous wave (CW) EPR imaging with direct detection and rapid field scan in the presence of rotating gradients

Sankaran Subramanian*[a], Janusz W. Koscielniak[b,a], Nallathamby Devasahayam[a], Ghadi Salem[c], Randall H. Pursley[c], Thomas J. Pohida[c], Murali C. Krishna[a]
[a]Radiation Biology Branch, Center for Cancer Research, National Cancer Institute, National Institutes of Health, Bethesda, MD 20892-1002, USA
[b]Signal Processing & Instrumentation Section, Center for Information Technology, National Institutes of Health, Bethesda, MD 20892, USA
[c]SAIC–Frederick NCI Cancer Research and Development Center, Frederick, MD 21224 USA

## ABSTRACT

The work described in this presentation relates to a novel approach to Electron Paramagnetic Resonance imaging *in vivo*. The method employs a continuous wave approach to spectral detection without the conventional low frequency modulation and phase sensitive detection. A combination of direct detection and rapid field scan in the simultaneous presence of rotating gradients enables imaging with high temporal resolution. Since CW detection is not limited to free radical spin probes with narrow spectral lines, unlike the time-domain case, this novel approach uniquely accomplishes ultra fast functional imaging and is applicable to common redox-sensitive spin probes without line-width restriction.

**Keywords**: CW EPR, imaging, Magnetic Resonance, rapidscan, rotating gradients

## INTRODUCTION

A major milestone in diagnostic non-invasive imaging is the discovery of magnetic resonance imaging (MRI),[1] which followed within a couple of decades of the discovery of the underlying physical phenomenon, namely, nuclear magnetic resonance spectroscopy(NMR).[2,3] Here, using radio frequency (RF) radiation in the presence of a strong magnetic field and superposed field gradients, one looks at the three dimensional (3D) distribution of nuclear spins, most commonly that of water protons in biological systems, to generate anatomical images in a non-invasive manner. The possibility of producing contrast in the images using the relaxation times $T_1$ and $T_2$ leads to clearly delineated images of organs with specific pathological conditions. This has led to the development of the so-called functional imaging protocols that not only provide anatomical details, but also contain physiological information. Such functional or physiological imaging techniques in biomedical research are receiving increased attention.

Among the recent methodologies in functional imaging which are receiving attention, the one based on Electron Paramagnetic Resonance (EPR),[4,5] a technique almost identical in principle and practice to NMR, has very promising applications in clinical investigations. EPR detects species with unpaired spins. In a given magnetic field, the frequency of an ensemble of unpaired electrons is 658 times that of the protons. There are two approaches for EPR imaging (EPRI) namely the continuous wave (CW) approach (constant frequency with a field sweep) or the time-domain (referred often to as Fourier transform: FT) modality (acquisition of impulse response of the system at constant field, followed by Fourier transform) [6]. EPRI using the CW methodology developed chronologically earlier than time-domain EPRI. This is because of

Design and Quality for Biomedical Technologies II, edited by Ramesh Raghavachari, Rongguang Liang, Proc. of SPIE Vol. 7170, 717008

the ultra fast spin dynamics of the ensemble of unpaired electrons and the need for very special electronic components and devices that are necessary to parallel the advances in MRI.

There are no stable free radicals of adequate concentration or biological half-life that occur naturally *in vivo*. Therefore, unlike MRI, EPR imaging would involve prior intravenous or intramuscular infusion of stable or slowly metabolizable non-toxic water-soluble free radicals, or stable implantable particulate spin probes, into the imaging subject. The National Cancer Institute at NIH (as well as many research groups) have been developing both the CW and pulsed EPR imaging methods with a special emphasis to use such an imaging modality in non-invasively probing tissue oxygen levels in tumors and to interrogate tissue redox status.[7-21] This is because most paramagnetic molecules are subject to oxygen broadening (oxygen itself being a paramagnetic molecule with two unpaired electrons, a ground state triplet), and a spatially resolved mapping of oxygen linewidth can provide quantitative evaluation of *in vivo* tissue oxygen levels. This would require perfusing the system with stable non-toxic free radicals. The use of FT methods in EPRI requires the availability of stable non-toxic free radicals with a very narrow spectral linewidth. This is because the spectral linewidth is inversely related to the transverse relaxation time ($T_2$) and hence the length of persistence of the response following an impulse. Normal spin probes used in EPR imaging such as nitroxyls have linewidths on the order of 0.1 mT with relaxation times in the sub-microsecond range. These are not suitable for time-domain imaging, although such nitroxyls are very sensitive to *in vivo* redox status. For example, stable nitoxyls, which are paramagnetic, gives a three-line EPR spectrum, and undergoes reduction to hydroxylamine or oxidation to oxammonium species.[22-24] Both the reduced and oxidized species are diamagnetic and are EPR-silent. Therefore, EPRI of nitroxyls *in vivo* can provide information on tissue redox status in specific anatomical locations and quantitative information of oxygen distribution in tumors. Since the linewidths of most paramagnetic species show quantitative dependence on the oxygen content if we can evaluate the spatially resolved linewidth of the paramagnetic spin probes, we can quantify *in vivo* oxygen concentration.

Tumors become hypoxic because new blood vessels are aberrant and support poor flow patterns.[25] Although tumors induce angiogenesis, the blood vessels that form are structurally and functionally abnormal, resulting in marked regional heterogeneity in tumor perfusion. As a result, tumor progression is paradoxically associated with both angiogenesis and hypoxia.[26] Longitudinal oxygen gradients in tumors result from lack of redundant arteriolar network leading to diffusion-limited hypoxia.[27] Fluctuations in red blood cell flux can cause intravascular oxygen to vary, causing hypoxia-reoxygenation.[25] Instabilities of red blood cell flux may actually be the norm within tumors, leading to widespread instability in partial pressure of oxygen (oxygenation; pO2). Thus, vascular stasis may not be the only process underlying transient hypoxia. Tumors classified as radiobiologically hypoxic (pO2 < 10 mmHg) have been associated with poor treatment outcome[28,29]). Hypoxia has a profound impact on tumor behavior and efforts that use hypoxia to predict tumor treatment response are gaining importance. A priori knowledge of hypoxia is of significant value in treatment planning, such as the use of hypoxic cytotoxins and appropriate staging of radiotherapy.[30] Therefore, robust techniques that are capable of monitoring tissue oxygen status in live objects noninvasively and quantitatively will be useful in preclinical research and eventually in clinical use in oncology. This is the reason for the interest in developing EPR imaging techniques at the National Cancer Institute. The present approach allows the generation of EPR images using continuous wave (CW) EPR technique quite different from the conventional approach. In section 2 we describe the general procedure to generate EPR image data and the construction of images by filtered back projection, the limitations we face in this method and trace the various attempts to speed up the CW imaging. In section 3 we outline the current innovation along with a description of the instrumentation and the results from phantoms and preliminary results *in vivo*. We finally conclude with a discussion and future prospects of this method.

## 2. CW EPR IMAGING

In the early nineteen seventies, Lauterbur[1] showed that it is possible to encode the spatial distribution of proton spin distribution in biological objects by measuring the spectrum in presence of linear magnetic field gradients. By collecting the projection of spin distribution in two or three dimensions in presence of static linear vector gradients, it is possible to reconstruct the image in as many dimensions using the filtered back-projection technique[31-33] that is common to X-ray, ultrasound CT and PET. The gradients are applied in polar coordinates, and the resulting projections are then back-projected to generate image information in a Cartesian axis system. Early nuclear magnetic resonance imaging experiments were also carried out using this method. If it is necessary to generate additional spectral information in addition to spatial distribution of spins in the object, spectral-spatial imaging is performed, in which the additional virtual spectral dimension is created by a further variation in the magnitude of the space encoding gradient.[34-38] Spectral spatial imaging thus involves generation of a fair number of sets of image data and constitutes about 10 times additional imaging time.

Almost all EPR work prior to 1970 was exclusively carried out using CW X-band (9 GHz) spectrometers. The application of EPR spectroscopy to live objects and biospecimens has necessitated the reduction of the measurement frequency to the radio frequency regime for reasons of adequate penetration. Recently several papers have appeared in the *in vivo* study of biological specimens at CW L-band.[39-42] With CW EPR imaging at these low frequencies, it has been possible to probe paramagnetic species with large linewidths (1-5 G) and multiple lines. In CW EPR imaging experiments using these probes, spatial as well as spectroscopic images have been obtained and physiological status could be derived non-invasively.

### 2.1 Conventional CW EPR with low frequency modulation

In conventional CW EPR, one uses a monochromatic radiation, usually in the MW and RF region of the electromagnetic spectrum, and the resonance condition which corresponds to the absorption of a precise quantum of circularly polarized radiation energy that matches with the Larmor frequency is achieved by a slow sweep of the magnetic field. In the CW detection scheme,[43] a microwave or RF bridge circuit which acts as a precision reflectometer, is employed with one arm connected to the incident MW source, and a

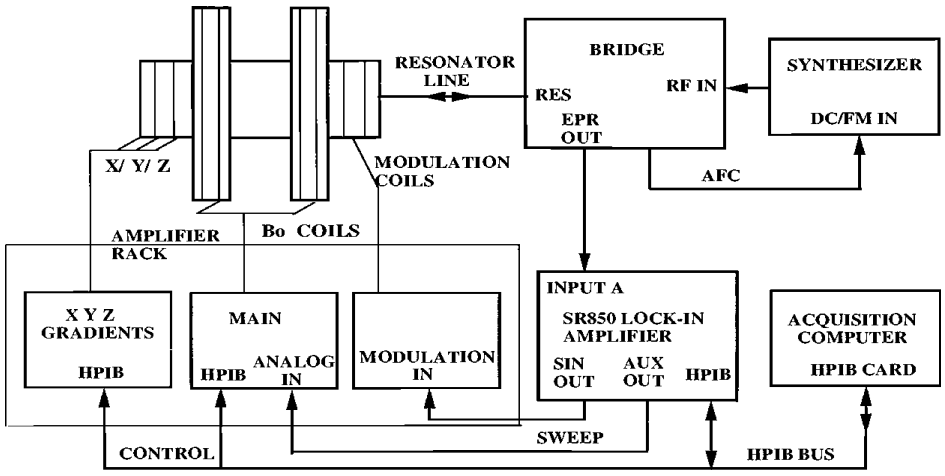


FIG. 1. Schematic diagram of 300 MHz continuos wave EPR imaging system showing the individual submodules consisting of Magnet, Gradient coil system, Analog Sweep unit, Modulation unit,RF bridge, RF synthesizer, SR850 lock-in amplifier, acquisition computer, and the communication links

second arm connected to a resonant cavity of appropriate dimensions, matched and tuned to the transmitter frequency. Under critical coupling conditions, when two of the bridge ports, one connected to the resonant cavity via a 50Ω transmission line and the other to a reference port, are exactly matched in impedance, there will be no energy transmission from the RF source to the signal detection port. Any mismatch produced by energy absorption brought about by resonance condition will produce a signal in the receiver port, which is proportional to differences in the return losses and the input power. In order to increase the sensitivity of detection the DC field is subjected to a low frequency modulation and the modulated output signals are detected in a phase-sensitive manner and amplified using a lock-in amplifier. Because the bridge circuit uses the imbalances produced by absorption of very low quantity of energy, it is imperative that the input frequency should be very stable, and a feed back automatic frequency control (AFC) circuit and an optional automatic coupling control circuit (ACC) preserve the frequency of the incident radiation unaltered during the passage through resonance.[44-46] These feedback controls, apart from correcting the frequency for any thermal drifts in the circuitry, also tend to correct frequency changes in the resonator due to the animal motion, when dealing with live animals. A schematic diagram of the 300 MHz CW spectrometer that we have designed[47] at the National Cancer Institute is shown in Fig. 1.

### 2.2 Limitations of field sweep rate in conventional CW EPR with low frequency modulation

Conventional EPR spectroscopy using low frequency modulation (10-100 kHz field modulation with amplitudes less than the linewidth of the paramagnetic spin probe) has the advantage of generating EPR signals at this modulation frequency and using a phase sensitive detector and lock-in amplifier that rejects all other signals including noise that are not at the modulation frequency, one achieves a high degree of sensitivity. The resulting signals appear as Lorentzian first derivative absorption or dispersion depending on the receiver phase. In this detection scheme it is not possible to increase the sweep rate arbitrarily. An accepted rule of thumb for sweep time is

$$\frac{sweep\ \ width}{Line\ \ width} \times \frac{Time\ \ const}{Sweep\ \ time} \langle\ 0.1$$

$$\text{i.e.} \qquad Time\,const < \frac{Sweep\,time \times Linewidth}{Sweep\,width} \times 0.01 \qquad [1]$$

In other words, for a paramagnetic probe with a linewidth of 0.02 to 0.1 mT, a sweep width of 1-2 mT and a receiver time constant of 1- 20 ms, the optimal sweep time is 1-100 sec. Faster sweep can lead to distortion in the line shape. This means that a typical projection may take 5 sec. and with about 144 projections needed for a 3D image, the measurement time is around 12 min. If we have to signal average by co-adding several scans per projection, then a 3D image may take an hour or so. During this time the spin concentration will change due to metabolism leading to unacceptable image intensity changes. It is therefore necessary to increase the speed of imaging by alternate data collection strategies. There have been two different attempts, one by Ohno et al.[48] and Deng et al.[49] which attempt to speed up the spatial encoding scheme without any change in the detection strategy, and the other by Joshi et al.[50] and Stoner et al.[51]where the detection scheme was changed to the so-called rapidscan sheme well known in NMR spectroscopy [52,53], where the signals were detected directly without any low frequency modulation and the field sweep was arbitrarily fast using triangular or sinusoidal sweeps superimposed on the Zeeman field corresponding to sweep rates on the order of T/sec.

### 2.3 Rotating gradients and the Rapidscan strategies for fast EPR imaging

Ohno et al. and Deng et al.[52,53] proposed an alternative imaging scheme in which the space-encoding gradients which are normally vector gradients rotated stepwise in two or three dimensions, were changed into a low frequency (4-10 Hz) rotating gradients and for each complete rotation of the gradients (by $2\pi$ radians) the field was kept constant, and then stepped to the next field position and the gradients were rotated again by $2\pi$, and so on. In other words, the entire projection data was gathered in a single sweep, with each field step being kept constant for a complete rotation of the gradient vector by $2\pi$. One can also

perform signal averaging by repeating the process a few times for improving the SNR. Once the signals are obtained, one has to reshuffle the resultant data to arrive at the conventional projections at each viewing angle before back projection. In fact such a strategy does speed up the imaging time by more than an order of magnitude, limited, however, by the modulation frequency and receiver filter time constant. In fact it will become easier to understand the rotating gradient strategy if one considers the matrix of projections versus gradient rotations as shown in Fig.2. Even with the slow sweep rate warranted by low frequency modulation, it is possible to obtain the projections at speeds better than 10 times the conventional mode. However, the projections are still obtained in the first derivative mode, and are to be integrated before performing filtered back-projection to generate the image data. Such a rotating gradient strategy indeed generates data much faster than the conventional slow sweep with individual projections being collected one at a time.


Fig.2 Schematic representation of a CW EPR two dimensional projection matrix. Let 8 projections be taken in 8 equally spaced orientations in a plane and let each projection be represented in 8 field steps, for simplicity. In the conventional slow sweep CW imaging the projections are gathered sequentially along the horizontal arrows each with constant angle θn and 8 field positions B1 to B8. In the case of Ohno et al. and Deng et al., the field is stepped in 8 steps and at each field position, the gradients completes one full rotation (θ1 to θ8), corresponding to the vertical arrows. After collecting the data, it is to be reshuffled by taking the first point in each of the field steps as the first projection, and the second in each field step constituting the second projection, and so on.

Joshi et al.[50] have employed the so-called 'rapidscan' strategy that was well known in NMR. In this scheme one does away with low frequency modulation of the Zeeman field, and directly detects the resonance signal by mixing the signal form the RF (MW) bridge with the transmitter frequency and detects the signal after amplification and after passing through a suitable low-pass filter. The absence of low frequency modulation allows very fast scans on the order of T/s. When the sweep rate becomes on the order or less than the inverse of the linewidth, one can see 'ringing' in the ESR signals[54] just as in high

resolution time domain response. While it may not be necessary to scan at such speeds, it is quite easy to remove the ringing pattern and correct the line shape by well-known Fourier deconvolution techniques commonly used in rapid scan correlation NMR and EPR spectroscopy[51-53]. It should be mentioned here that although the direct detection scheme is less sensitive than the one with low frequency modulation, it directly produces the absorption spectral profiles. In general, the amplitude of the absorption signal decreases in inverse proportion to the width of a signal, whereas that of a first derivative decreases in proportion to square of the width. Therefore, other things being equal, the absorption profiles are likely to show better dynamic range under large imaging gradients than the derivatives, making the rapid scan strategy more attractive. It has been shown that such a strategy indeed can generate EPR images quite fast compared to the conventional slow-sweep with low frequency modulation. The rapidscan CW EPR spectrometer is essentially the same as shown in Fig.1 without the modulation and lock-in amplifier. The signals from the bridge are mixed down to base band, amplified by a low noise low-frequency amplifier and digitized synchronously with the filed sweep. With a 10 kHz frequency of triangular sweep and an amplitude of about 1mT peak-to-peak superimposed on the main Zeeman field, one can easily accomplish a sweep rate of 2T/sec. (10 mT for every half-cycle period).

## 3. COMBINED RAPIDSCAN AND ROTATING GRADIENTS FOR ULTRA FAST EPR IMAGING

A third possibility in collecting the projections (elements of the Bθ matrix) in CW EPR will be the *simultaneous* rapid scanning of the sweep-field and a synchronous rotation of the gradients[10] represented by the diagonal arrow direction in Fig.2. To minimize the collection-time of projection data, we shall combine rapid scan and rotating gradients with direct detection. Considering the data collection strategy, if one looks along the diagonal of the matrix, it can be seen that both the field and the gradients synchronously increase. We perform one full sweep of the required region of the field by a rapid scan and digitize the projection signal in 64 or 128 steps (in Fig.2 it will be 8 steps) and simultaneously rotate the gradient vector through one full cycle (0 to $2\pi$ radians) in 128 steps. We collect the EPR signals with a fast digitizer, say, in 128steps. (In the simplified example of Fig.2 we would have collected the 8 matrix elements along the diagonal). We can follow this by scanning the field from high to low (this will be natural, since we will be performing the rapid scan either sinusoidally or using triangular sweeps so that in every cycle there will be a forward and a reverse sweep) still rotating the gradient from 0 to $2\pi$ radians. The detected signals will now fill the elements of the Bθ matrix along the anti-diagonal (right to left) from top to bottom. The other elements are to be filled along lines parallel to the diagonal or the anti-diagonal of the Bθ matrix, and in order to accomplish this we need to impart an incremental phase shift by $2\pi/n$ (in the simplified case of Fig.2 the phase shift will be $2\pi/8$) to the gradient rotation for each pair of upward and downward field scan. The data is collected in such a way that those from upward sweeps are stored separately from the ones from downward sweeps. What is required now is to shuffle the matrix such that the data parallel to the diagonals are reorganized to generate the conventional projection matrix. This is followed by a filtered back-projection to generate the images.

### 3.1 Instrumentation for rapidscan with rotating gradients

Our 300 MHz CW imaging spectrometer[17] that was used for conventional measurements with low frequency modulation, phase sensitive detection and constant vector gradients could be easily modified for the present work. The low frequency modulation coil was used to provide the rapid sinusoidal scan and was able to operate at 1.2 kHz using a Kepco 20 Amp. amplifier with little distortion. This enabled the application of a sinusoidal magnetic field over the Zeeman field that enabled rapid sweeps of up to 2.5 mT. A careful analysis of the amplitude pattern of the sine wave shows that 35% (±17.5%) of the amplitude centered about the sign-crossover mid point is linear with deviation from linearity being less than 0.4%. The time taken for sweeping this linear range is 35% of half the cycle period. It can be easily shown that very fast field scan on the order of several T/s is possible with each projection acquired in 104 μs. For the application of rotating gradients, the existing set of three orthogonal gradients (X, Y and Z) could be powered with a set of three Kepco amplifiers at a frequency of 4.8 kHz and maximum amplitude of ± 40 mT/m. Planar circularly polarized 2D gradients were generated by applying identical currents in two of the orthogonal coils (X & Y, X & Z, or Y & Z pairs) for two-dimensional imaging, and 3D gradients over a

sphere, by incorporating the third orthogonal coil generating tilted planes of rotating gradients for the sake of three-dimensional imaging.

### 3.2 Digital generation of waveforms for sinusoidal sweep and rotating gradients

The 1.2 kHz low-frequency rapid scan signal, the three higher frequency (4.8 kHz) gradient signals, and the trigger signals for data acquisition were generated using National Instruments LabView® software and National Instrument PCI-6289 multifunction data acquisition card. This card is capable of generating four independent 16-bit analog signals at a maximum voltage of 10 Vp-p and a maximum output rate of 2.8 MS/s. The card can also output up to 48 digital input/output signals. The phases of the three gradient signals can be altered programmatically relative to the phase of the rapid scan signal. For example, to acquire images parallel to the XZ plane, the X and Z gradient outputs are set 90 ° out of phase relative to each other and at 4.8 kHz frequency and the rapidscan sinusoidal sweep field was applied at 1.2 kHz. The amplitudes of the gradient signals are carefully adjusted to result in a circularly polarized gradient field rotating in the XZ plane at the selected frequency. The phase of the X and Z gradients can then be incremented relative to the rapid scan field at any desired step interval. Using a digital signal processing transmitter module it was possible to generate programs for two and three dimensional data acquisition with rotating gradients with 64 or 128 phase-steps and sinusoidal sweeps as well as timing pulses for acquisition triggers. The LabView software also allowed acquisition of EPR signals and summing them in real time for signal averaging. This is represented in Fig.3.

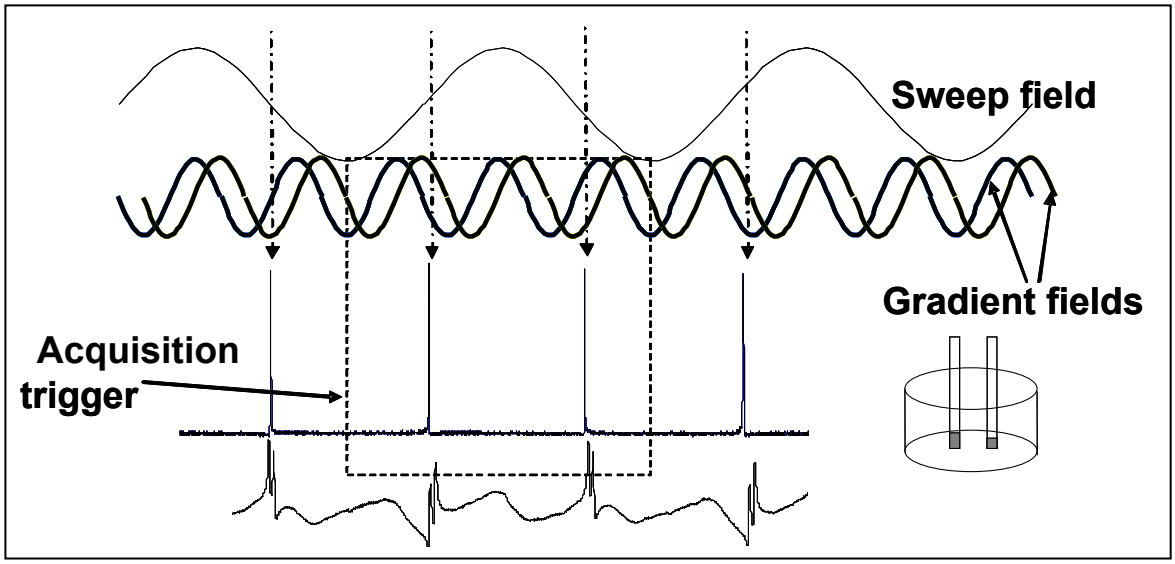


Fig.3 Direct detected absorption EPR signals of a phantom sample (shown on the left: two tubes of 2mM trityl radicals) with and without gradients. The top sinusoid represents the rapid scan sweep (1.2 kHz) , and the two high frequency sinusoids (4.8 kHz) represent the X and Z gradients, which together provide the rotating gradient in the XZ plane. The left side of the dotted rectangle represents the start of the trigger. 64 samples at 600 kS/s were collected for each gradient phase setting, giving rise to one downfield scan and one up field scan (second). In presence of gradients, each of the spectral lines is split into two (the bottom projections profile) due to spatial encoding. The rotating gradients also lead to a rolling background. This can be eliminated by taking back-ground signal with the central field offset away from resonance and subtracting the same from the one obtained with the field set on resonance.

The relative positioning of the gradient and the sweep sinusoids allow a full cycle ($2\pi$ radians) of gradient rotation at the middle of the positive-going and also in the negative-going sweeps, generating two 'pseudo' projections per sweep sinusoid. This can be repeated, and the entire signal under each full rotation of the gradient cycle is sampled in 64 (or 128) steps. After averaging the necessary number of pseudo-projections at a constant phase of the gradients, the gradient phases are digitally shifted by $2\pi/64$ (or $2\pi/128$) and the collections continued. The resulting 64 x 64 (or 128 x 128) projection matrix constitutes a skewed 2D 'pseudo' sinogram, which can be un-skewed by shuffling the matrix (see Fig.2) to generate the conventional sinogram followed by filtered back-projection to yield the image. Simulation of the conventional as well as rapidscan-rotating gradient sinograms and the images obtained by back projection

are given in Fig. 4. For 3D collection, all that is to be done is to apply the combination of the three sinusoidal gradients such that they will represent a series (usually 64) of 2D experiments with the 2D rotating gradient planes progressively tilted about the polar axis in steps of $2\pi/64$ over a total span of $0\text{-}2\pi$ radians. The resulting data is sequentially shuffled and back-projected in two steps to generate the 3D image. With the current frequencies of the sweep and gradients we are able to generate data almost as fast as in time-domain EPR! (See Table I)

Table I CW Rapidscan-Rotating gradient direct detection measurement times

| | |
|---|---|
| 1D Single 64 point projection | 208 μs |
| 2D image 64x64 points | 52.4 ms |
| 3D image 64x64x64 points | 3.35 s |

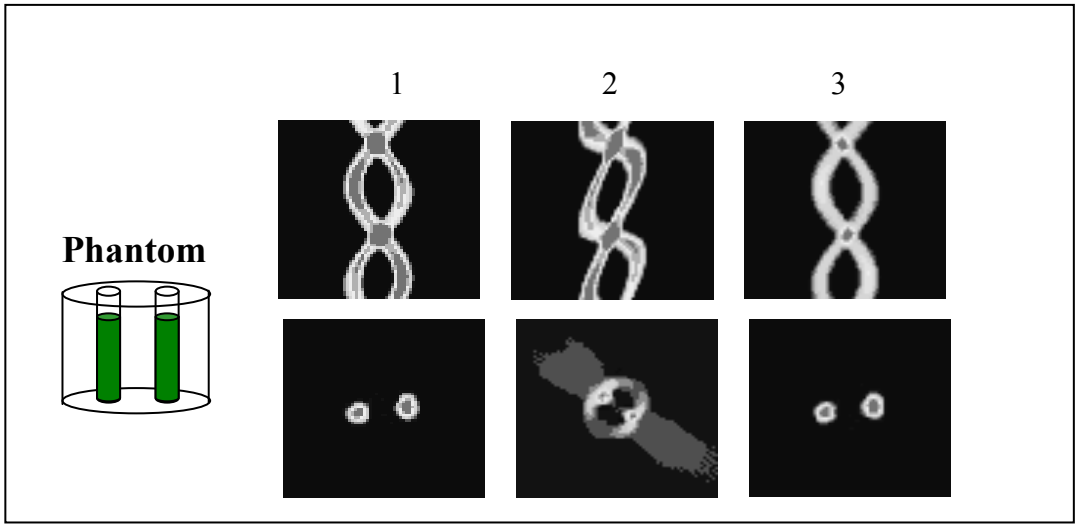


Fig.4 Conventional sinogram from a 2-tube phantom (on the left) and the corresponding filtered back-projected image (column 1). Skewed pseudo sonogram and the corresponding pseudo image as obtained from the raw data when projections were collected with simultaneous sweep and rotating gradients (column 2). Reshuffling the matrix leads to the correct sinogram and the expected image (column 3).

### 3.3 Results of rapidscan rotating gradient CW EPR imaging

Although the speed of the sinusoidal field scan as well as the gradient rotating frequency have not yet been optimized for want of suitable AC amplifiers and low inductance coils for both, our preliminary results are indeed promising. The existing instrument automation allows the selection of the gradient amplitude, the 2D plane (XY, XZ or YZ) and the number of projections (64 or 128) which also represent the phase shifts between rapidscan acquisitions. Before the start of the actual imaging experiment, the gradient free spectrum is monitored and the maximum and minimum of the Zeeman field is ascertained for which the spectrum just disappears at either extreme of the field range generated by the sinusoidal rapid scan. Placing the Zeeman field right at the middle of the two values will position the center of the linear region of the sweep at the center of the projections. Once this id done then the computer based image data collection takes over the data collection. Once the number of averages, the number projections and gradient magnitudes are selected, a dummy scan is performed with the magnetic field offset far away from the signal and stored as set of background data for each orientation of the gradient vector. This is followed by the actual measurement of the projections with the Zeeman field brought to its central location. The program collects the data, performs background subtraction, performs filtered back-projection and displays the image on the monitor, continuously after each measurement. With 2 mM trityl solution and with 5 averages it was possible to generate back-projected phantom image data every 200 ms. which is as fast as image data generation in time-domain EPR imaging. Fig. 6 shows the graphic user interface (GUI) that allows the 2D and 3D data collection, selects the particular measurement parameter set, the number of averages, option for baseline correction, etc. Every time the measurement is over (few seconds at the most

for 2D imaging) the GUI shows the selected projection for the forward and reverse sweeps and the corresponding back-projected images. The GUI also displays the overall time taken for each measurement. It also automatically saves the projection and image data. With this arrangement it would be possible to examine 2D images of small animals *in vivo* almost as fast as in MRI. In the example shown in Fig. 6, the phantom consisted of 3 tubes of 6 mm i.d. filled with 500 μL of 2 mM Oxo63 in water. The number of averages was 100 (5 averages gave adequate SNR) and the total time for measurement & back-projection was 10 sec.

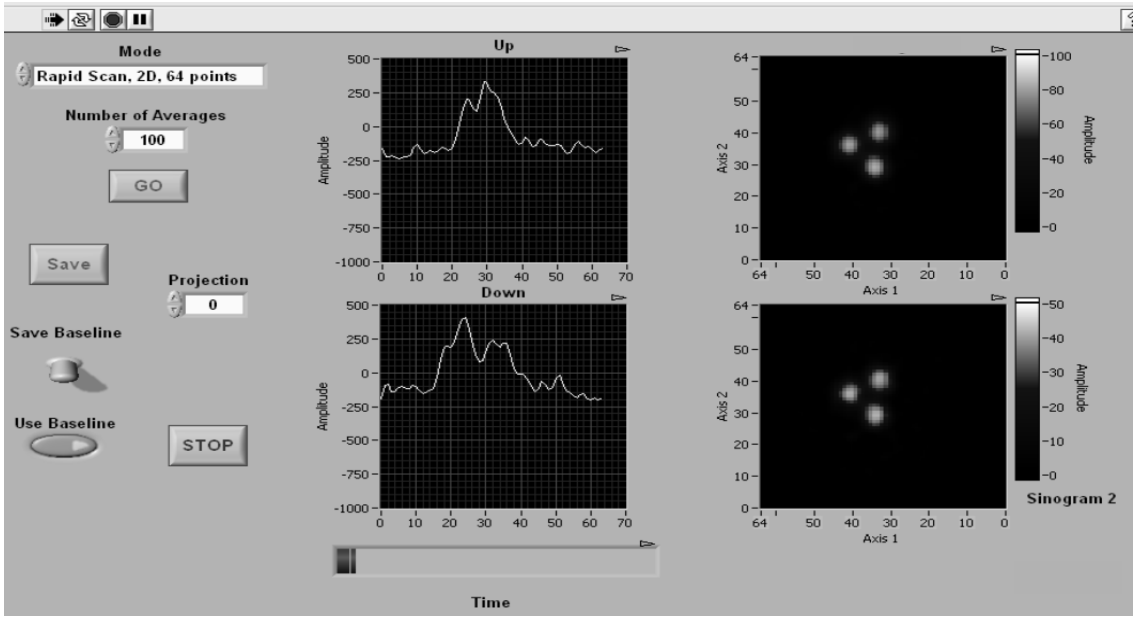


Fig. 5. Screen-shot of our rapid-scan rotating gradient GUI (graphic use interface) that allows the automation of CW EPR imaging. Selection of the imaging parameters (2D or 3D) along with the number of projections, gradient magnitudes, etc. are already programmed into EPROM in the digital transmit module as a set of numbered experiments. The number of averages, base-line corrections etc. can be entered through front panel. The GUI also presents the images for both the forward and reverse scans from the sinusoidal sweeps. The software is based on LabView® platform and controls the setting up of the experiment, instrument control, acquisition of data and data post-processing to generate back-projected images.

We have also carried out in 3D vivo studies on mouse tumor models. Our preliminary results indicate that 3D data sets with 64 azimuthal and 64 polar angular increments corresponding to a total of 4096 projections with 10 averages for each projection can be carried out in 67 sec. Fig. 7 shows a surface-rendered mouse-tumor image from a 3D CW rapidscan-rotating gradient experiment with 4096 projections obtained in 1 min. The mouse tumor imaging experiments were carried out according the approved NCI protocol as has been detailed in our previous publications.[55-58]

## 4. DISCUSSION

Results obtained in this work on the phantoms and *in vivo* clearly demonstrate the novelty of the simultaneous rapid scan and field gradient rotation in CW EPR imaging. It is indeed gratifying to note that CW EPR imaging can be performed at speeds that match that of time-domain methods using this strategy. Spin probes that are sensitive to redox status in tissues, such as nitroxyls, have large linewidths (around .1 to 0.2 mT) and are not amenable for pulsed EPR investigations at low frequencies because of the very short transverse relaxation time. Fortunately, CW EPR is not limited by the linewidth of the spin probe, and the application of the current approach will be capable of providing the required temporal resolution in

investigating treatment responses and spatially resolved redox kinetics both *in vivo* and in vitro with considerable accuracy compared to the conventional EPR imaging with low frequency modulation.

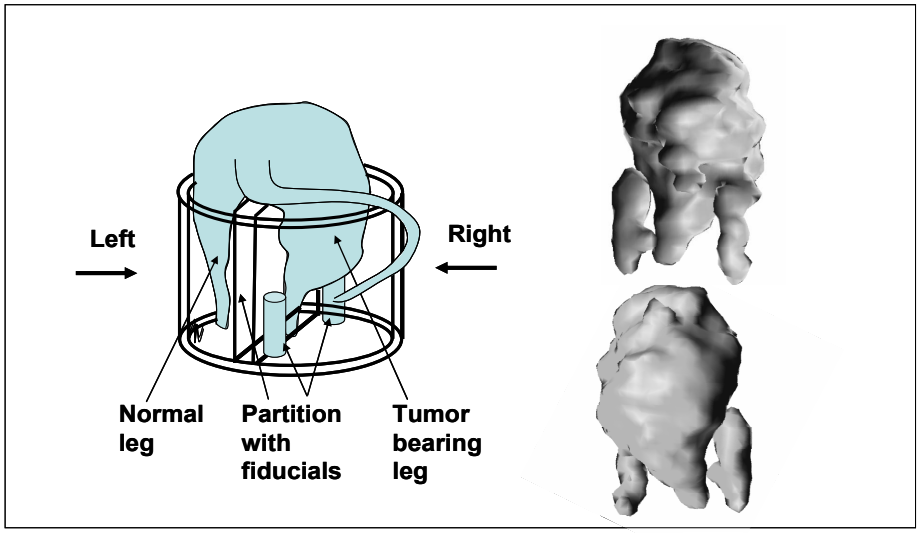


Fig. 6 First example of a 3D *in vivo* EPR imaging using the rapidscan combined with rotating gradient. The tumor-bearing and normal legs of a C3H mouse were placed in a 25 mm cylindrical resonator. Two small tubes (4 mm i.d.) containing 200 μL of 2 mM oxo63 were placed as fiducials on either side of the tumor-bearing leg. After infusing the trityl radical (Oxo63) through tail-vein cannulation so as to have average blood concentration of 2 mM, 4096 projections were obtained (64 polar angular increments of gradient planes and for each of this 64 azimuthal increments of gradient orientations ). These were used to reconstruct the 3Diamges via a two-stage filtered back-projection. Surface rendered 3D images seen on the left for two perspectives faithfully reproduce the spin distribution. Imaging time is 67 sec.

There are several improvements over the current specifications. We have not fully examined the availability of low noise AC amplifiers required for the generation of rotating gradients. Our existing gradient coil system is not the ideal one for higher frequency operation. There could be design aspects and coil materials (Litz wire, for example) that may lead to lower inductances and minimum distortions of the waveforms. Once could also think of triangular sweeps, and recently circuits have been designed to generate highly linear, triangular sweeps ideal for rapid scan experiments. Solenoidal resonators may act as good antenna for the oscillatory gradients and will lead to sinusoidal base-line artifacts (as has been seen in the bottom projection taken under the rotating gradients, in Fig. 3. The baseline roll can, however, be eliminated by performing the experiment under identical conditions with the field off-set away from resonance and subsequently subtracting the baseline, giving neat projections with flat base-lines. We have not tried other type of resonators, such as loop-gap resonator which may not be susceptible for such large pick-ups from the oscillatory gradients. The scan speed needs to be optimized keeping in mind the increased bandwidth to be detected due to the rapid scan, as well as the increased presence of FID-like ringing artifacts, although the latter can be removed by Fourier deconvolution methods.[50,52,53] It is almost certain that too fast a scan speed that will introduce FID-like ringing (and hence will require removal by Fourier deconvolution) will hardly be needed in view of the gradient induced broadening, although the scan speed can be several orders of magnitude faster than that employed in conventional low frequency modulation. This will enable rapid CW EPR imaging.

Another important factor is that for CW measurements one needs much less RF/MW power (on the order of mW) even taking into account of the duty cycle, and as such the ultra fast CW EPR imaging using the current strategy should have SAR far less than what is allowed by FDA. When all precautions are taken into account it may be possible to produce CW EPR images at speeds that match with time-domain methods that may use RF power levels that are several orders of magnitude lower. The availability of non-

toxic spin probes such as those based on trityl radical coupled with this low power ultra fast EPR imaging mode will make CW EPR quite a viable approach for quantitative estimate of tissue oxygenation, temporally well-resolved estimates of redox status and investigations of tumor physiology in an *in vivo* setting. Another application is in radiation dosimetry,[59-61] where one has to quantitatively assess the spin count of radicals generated in tooth enamels of persons accidentally exposed to high energy radiations. Since this involves weak signals with broad linewidths, and pulsed methods are out of question, the current strategy is by far the most efficient approach, especially when a high throughput is required in dealing with large number of patients.

It will of course be important to optimize the various parameters (frequency of the gradients and sweep) and use the most modern digital signal processing tools. Once this is done, it will be possible to compare the various approaches of CW EPR imaging and the pulsed modes. Only then can we make the right choice of the imaging modality in a given situation.

## 5. ACKNOWLEDGEMENTS

This research was supported by the Intramural Research Program of the NIH, Center for Cancer Research, National Cancer Institute.

## 6. REFERENCES

[1] Lauterbur, P. C. "Image Formation by Induced Local Interactions: Examples Employing Nuclear Magnetic Resonance", Nature, 242, 190-191.(1973)

[2] Bloch, F., Hansen, W. W., Packard, H. E. "Nuclear Induction", Phys. Rev., 69, 127-131.(1946)

[3] Purcell, E. H., Torrey, H. C., Pound, R. V. "Resonance absorption by nuclear moments in solid", Phys. Rev., 69, 37-38.(1946)

[4] Eaton, G. R., Eaton, S. E., Ohno, K., editors. [EPR imaging and in vivo EPR] Boca Raton, CRC Press; 1991.

[5] .Zavoisky, E. "Spin-magnetic resonance in paramagnetics", J. Phys. E., 9, 245-249.(1945)

[6] Ernst, R. R., Anderson, J. R. "Application of Fourier spectroscopy to nuclear magnetic resonance", Rev Sci Instrum, 37, 93-102.(1966)

[7] Bourg, J., Krishna, M. C., Mitchell, J. B., Tschudin, R. G., Pohida, T. J., Friauf, W. S., Smith, P. D., Metcalfe, J., Harrington, F., Subramanian, S. "Radiofrequency FT EPR Spectroscopy and Imaging", J. Magn. Reson. B, 102, 112-115.(1993)

[8] Murugesan, R., Afeworki, M., Cook, J. A., Devasahayam, N., Tschudin, R., Mitchell, J. B., Subramanian, S., Krishna, M. C. "A broadband pulsed radio frequency electron paramagnetic resonance spectrometer for biological applications", Rev. Sci. Instrum., 69, 1869-1876.(1998)

[9] Murugesan, R., Cook, J. A., Devasahayam, N., Afeworki, M., Subramanian, S., Tschudin, R., Larsen, J. A., Mitchell, J. B., Russo, A., Krishna, M. C. "In vivo imaging of a stable paramagnetic probe by pulsed-radiofrequency electron paramagnetic resonance spectroscopy", Magn. Reson. Med., 38, 409-414.(1997)

[10] Subramanian, S., Koscielniak, J. W., Devasahayam, N., Pursley, R. H., Pohida, T. J., Krishna, M. C. "A new strategy for fast radiofrequency CW EPR imaging: Direct detection with rapid scan and rotating gradients", J. Magn. Reson., 186, 212-219.(2007)

[11] Subramanian, S., Matsumoto, K. I., Mitchell, J. B., Krishna, M. C. "Radio frequency continuous-wave and time-domain EPR imaging and Overhauser-enhanced magnetic resonance imaging of small animals: instrumental developments and comparison of relative merits for functional imaging", Nmr in Biomedicine, 17, 263-294

(2004)

[12] Subramanian, S., Mitchell, J. B., Krishna, M. C., "Time-domain radio frrquerncy EPR imaging", Biological Magnetic Resonance, Berliner, L. J., ed.,Kluwer Academic, New York, pp. 153-197 (2003)

[13] Subramanian, S., Murugesan, R., Devasahayam, N., Cook, J. A., Afeworki, M., Pohida, T., Tschudin, R. G., Mitchell, J. B., Krishna, M. C. "High-speed data acquisition system and receiver configurations for time-domain radiofrequency electron paramagnetic resonance spectroscopy and imaging", J. Magn. Reson., 137, 379-388.(1999)

[14] Alecci, M., Dellapenna, S., Sotgui, A., Testa, L., Vannucci, I. "Electron-Paramagnetic Resonance Spectrometer for 3-Dimensional Invivo Imaging at Very Low-Frequency", Rev. Sci. Instrum., 63, 4263-4270 (1992)

[15] Halpern, H. J., Spencer, D. P., van Polen, J., Bowman, M. K., Nelson, A. C., Dowey, E. M., Teicher, B. A. "Imaging radio frequency electron-spin-resonance spectrometer with high resolution and sensitivity for in vivo measurements", Rev. Sci. Instrum., 60, 1040-1050.(1989)

[16] Halpern, H. J., Yu, C., Peric, M., Barth, E., Grdina, D. J., Teicher, B. A. "Oximetry deep in tissues with low-frequency electron paramagnetic resonance", Proc. Natl. Acad. Sci. USA, 91, 13047-13051.(1994)

[17] Koscielniak, J., Devasahayam, N., Moni, M. S., Kuppusamy, P., Yamada, K., Mitchell, J. B., Krishna, M. C., Subramanian, S. "300 MHz continuous wave electron paramagnetic resonance spectrometer for small animal in vivo imaging", Rev. Sci. Instrum., 71, 4273-4281.(2000)

[18] Kuppusamy, P., Ohnishi, S. T., Numagami, Y., Ohnishi, T., Zweier, J. L. "3-Dimensional Imaging of Nitric-Oxide Production in the Rat-Brain Subjected to Ischemia-Hypoxia", J Cerebr Blood F Met, 15, 899-903.(1995)

[19] Liu, K. J., Gast, P., Moussavi, M., Norby, S. W., Vahidi, N., Walzak, T., Wu, M., Swartz, H. M. "Lithium phthalocyanine: a probe for electron paramagnetic resonance oximetry in viable biologic systems", Proc. Natl. Acad. Sci. USA, 90, 5438-5442.(1993)

[20] Quine, R., Rinard, G. A., Eaton, S. S., Eaton, G. R. "A Pulsed and Continuous Wave 250 MHz Electron Paramagnetic Resonance Spectrometer", Conc. Magn. Reosn., 15, 59-91.(2002)

[21] Utsumi, H., Takeshita, K., Miura, Y., Masuda, S., Hamada, A. "In vivo EPR measurement of radical reaction in whole mice - influence of inspired oxygen and ischemia-reperfusion injury on nitroxide reduction", Free. Rad. Res. Comm., 19, S219-227.(1993)

[22] .Krishna, M. C., Grahame, D. A., Samuni, A., Mitchell, J. B., Russo, A. "Oxoammonium Cation Intermediate in the Nitroxide-Catalyzed Dismutation of Superoxide", Proc. Natl. Acad. Sci. USA, 89, 5537-5541.(1992)

[23] Kuppusamy, P., Li, H. Q., Ilangovan, G., Cardounel, A. J., Zweier, J. L., Yamada, K., Krishna, M. C., Mitchell, J. B. "Noninvasive imaging of tumor redox status and its modification by tissue glutathione levels", Cancer Res, 62, 307-312.(2002)

[24] Kuppusamy, P., Li, H. Q., Ilangovan, O., Cardounel, A. J., Zweier, J. L., Mitchell, J. B. "In vivo imaging of tumor redox status: Effect of GSH depletion", Free Radical Bio Med, 31, S139-S139.(2001)

[25] Lanzen, J., Braun, R. D., Klitzman, B., Brizel, D., Secomb, T. W., Dewhirst, M. W. "Direct demonstration of instabilities in oxygen concentrations within the extravascular compartment of an experimental tumor", Cancer Res., 66, 2219-2223.(2006)

[26] Dewhurst, M. W., Navia, I., C., Brizel, D. M., Willett, C., Secomb, T. W. "Multiple Etiologies of Tumor Hypoxia Require Multifaceted Solutions ", Clin. Cancer Research, 13, 375-377.(2007)

[27] Dewhirst, M. W., Ong, E. T., Braun, R. D., Smith, B., Klitzman, B., Evans, S. M., Wilson, D. "Quantification of longitudinal tissue pO(2) gradients in window chamber tumours: impact on tumour hypoxia", Br. J. Cancer, 79, 1717-1722.(1999)

[28] Hockel, M., Vaupel, P. "Tumor hypoxia: Definitions and current clinical, biologic, and molecular aspects", J. Natl. Cancer. Inst.,93, 266-276.(2001)

[29] Hockel, M., Schlenger, K., Aral, B., Mitze, M., Schaffer, U., Vaupel, P. "Association between tumor hypoxia and malignant progression in advanced cancer of the uterine cervix", Cancer Res.,56, 4509-4515.(1996)

[30] Brown, J. M., Giaccia, A. J. "The unique physiology of solid tumors: Opportunities (and problems) for cancer therapy", Cancer Res.,58, 1408-1416 (1998)

[31] Bracewell, R. N.,[Two Dimensional Imaging] Prentice Hall, New York, (1994)

[32] Kak, A. C., Slaney, M., [Principles of computerized tomographic imaging] IEEE Press. New York, (1988)

[33] Natterer, F., [The mathematics of computerized tomography]. Wiley. Chichester (1986).

[34] Eaton, G. R., Eaton, S. S., Maltempo, M. M. "3 Approaches to Spectral Spatial Epr Imaging", Appl. Radiat. Isotopes, 40, 1227-1231.(1989)

[35] Ewert, U., Herrling, T. "Spectrally resolved EPR tomography with stationary gradient", Chem. Phys. Lett., 129, 516-520.(1986)

[36] Lauterbur, P. C., Levin, D. N., Marr, R. B. "Theory and Simulation of Nmr Spectroscopic Imaging and Field Plotting by Projection Reconstruction Involving an Intrinsic Frequency Dimension", J. Magn. Reson., 59, 536-541.(1984)

[37] Maltempo, M. M. "Differentiation of spectral and spatial components in EPR imaging using 2-D image reconstruction algorithms", J. Magn. Reson., 69, 156-163.(1986)

[38] Maltempo, M. M., Eaton, S. S., Eaton, G. R. "Spectral-spatial two dimensional EPR imaging", J. Magn. Reson., 72, 449-455.(1987)

[39] Kuppusamy, P., Chzhan, M., Wang, P. H., Zweier, J. L. "Three-dimensional gated EPR imaging of the beating heart: Time-resolved measurements of free radical distribution during the cardiac contractile cycle", Magn. Reson Med, 35, 323-328.(1996)

[40] Ohara, J. A., Goda, F., Liu, K. J., Bacic, G., Hoopes, P. J., Swartz, H. M. "The pO2 in a Murine Tumor after Irradiation - an in-vivo Electron-Paramagnetic-Resonance oximetry study", Radiat. Res., 144, 222-229.(1995)

[41] Swartz, H. M., Clarkson, R. B. "The measurement of oxygen in vivo using EPR techniques", Phys. Med. Biol.,43, 1957-1975.(1998)

[42] Zweier, J. L., Wang, P. H., Kuppusamy, P. "Direct Measurement of Nitric-Oxide Generation in the Ischemic Heart Using Electron-Paramagnetic-Resonance Spectroscopy", J. Biol. Chem., 270, 304-307.(1995)

[43] Poole, C. P., Electron Spin Resonance: [A Comprehensive Treatise on Experimental Techniques]. John Wiley & Sons. New York,(1997).

[44] Hirata, H., Fujii, H. "Automatic matching control circuit based on phase-sensitive detection for in vivo CW-EPR spectroscopy", Meas. Sci. Tech.,18 N27-N31.(2007)

[45] Hirata, H., Luo, Z. W. "Stability analysis and design of automatic frequency control system for in vivo EPR spectroscopy", Magn. Reson. Med., 46, 1209-1215.(2001)

[46] Hirata, H., Walczak, T., Swartz, H. M. "An improved inductive coupler for suppressing a shift in the resonance frequency of electron paramagnetic resonance resonators", Rev. Sci. Instrum., 68, 3187-3191.(1997)

[47] Koscielniak, J., Devasahayam, N., Moni, M. S., Kuppusamy, P., Yamada, K., Mitchell, J. B., Krishna, M. C., Subramanian, S. "300 MHz continuous wave electron paramgnetic resonace spectrometer for small animal in vivo imaging", Rev Sci Instrum, 71, 4273-4281.(2000)

[48] Ohno, K., Watanabe, M. "Electron paramagnetic resonance imaging using magnetic-field-gradient spinning", J Magn Reson, 143, 274-279.(2000)

[49] Deng, Y. M., He, G. L., Petryakov, S., Kuppusamy, P., Zweier, J. L. "Fast EPR imaging at 300 MHz using spinning magnetic field gradients", J. Magn. Reson., 168, 220-227.(2004)

[50] Joshi, J. P., Ballard, J. R., Rinard, J. A., Quine, R. W., Eaton, S. S., Eaton, R. R. "Rapid-scan EPR with triangular scans and Fourier deconvolution to recover the slow-scan spectrum", J. magn. Reson., 175, 44-51.(2005)

[51] Stoner, J. W., Szymanski, D., Eaton, S. S., Quine, R. W., Rinard, G. A., Eaton, G. R. "Direct-detected rapid-scan EPR at 250 MHz", J. Magn. reson., 170, 127-135 (2004)

[52] Dadok, J., Sprecher, R. F. "Correlation Nmr-Spectroscopy", J. Magn. Reson., 13 243-248.(1974)

[53] Gupta, R. K., Ferretti, J. A., Becker, E. D. "Rapid Scan Fourier-Transform Nmr-Spectroscopy", J. Magn. Reson., 13, 275-290.(1974)

[54] Czoch, R., Francik, A., Indyka, J., Koscielniak, J., EPR, 41-43., M. A. C. "EPR spectrometer with rapid scan", Meas. Automatic Contr., 29, 41-43.(1983)

[55] Matsumoto, K., English, S., Yoo, J., Yamada, K., Devasahayam, N., Cook, J. A., Mitchell, J. B., Subramanian, S., Krishna, M. C. "Pharmacokinetics of a triarylmethyl-type paramagnetic spin probe used in EPR oximetry", Magn. Reson. Med., 52, 885-892.(2004)

[56] Matsumoto, K., Subramanian, S., Devasahayam, N., Aravalluvan, T., Murugesan, R., Cook, J. A., Mitchell, J. B., Krishna, M. C. " Electron paramagnetic resonance imaging of tumor hypoxia: enhanced spatial and temporal resolution for in vivo pO2 determination ", Magn. Reson. Med., 55, 1157-1163.(2006)

[57] Matsumoto, K., Thirumaran, A., Chandrika, B., Devasahayam, N., Cook, J. A., Mitchell, J. B., Subramanian, S., Krishna, M. C. "In vivo electron paramagnetic resonance oxymetry: Comparison of continuous wave and pulsed techniques", Free Rad. Biol. Med.,35,(2003)

[58] Matsumoto, S., Hyodo, F., Subramanian, S., Devasahayam, N., Munasnghe, J., Hyodo, E., Gadisetti, C., Cook, J. A., Mitchell, J. B., Krishna, M. C. "Low-field paramagnetic resonance imaging of tumor oxygenation and glycolytic activity in mice", J. Clin. Invest., 118, 1965-1973.(2008)

[59] Guttler, A., Wieser, A. "EPR-dosimetry with tooth enamel for low doses",Rad. Meas., 43, 819-822.(2008)

[60] Wieser, A., Fattibene, P., Shishkina, E. A., Ivanov, D. V., De Coste, V., Guttler, A., Onori, S. "Assessment of performance parameters for EPR dosimetry with tooth enamel", Rad. Meas., 43, 731-736.(2008)

[61] Simon, S. L., Bailiff, I., Bouville, A., Fattibene, P., Kleinerman, R. A., Lloyd, D. C., McKeever, S. W. S., Romanyukha, A., Sevan'kaev, A. V., Tucker, J. D., Wieser, A. "BiodosEPR-2006 consensus committee report on biodosimetric methods to evaluate radiation doses at long times after exposure", Rad. Meas., 42, 948-971.(2007)